 Bull. Chem. Soc. Jpn., 75, 1111–1118 (2002)

Polarization Specific Ultrafast Nuclear Dichroic Responses: Raman Spectral Density Recovery and Coherent Coupling Effects

Lawrence D. Ziegler,* Jian Peng, and Steven Constantine

Department of Chemistry, Boston University, Boston MA 02215, USA

(Received November 12, 2001)

The frequency selected dichroic ultrafast responses of neat carbon tetrachloride are reported as a function of pump and probe polarization orientations in a standard two beam experimental configuration. The recovery of the Raman spectral density from these experimental observations is demonstrated. The influence of coherent coupling effects, in this one color, electronically nonresonant class of ultrafast pump–probe experiments is considered. While their contribution to Raman spectral densities via birefringent observations can be neglected, these terms can only be eliminated from the dispersed dichroic technique for Raman spectral density recovery when two-color pump–probe studies are performed.

Measurements of polarization specific Raman spectra can provide considerable information regarding the symmetry, scattering mechanism and relaxation process for these polarizability coupled nuclear degrees of freedom. In particular, time domain experimental techniques based on the impulsive excitation due to femtosecond pulses are conveniently well-suited for the study of Raman spectral densities associated with intermolecular degrees of freedom in condensed phase samples.[1–5] The original two-beam optical heterodyne detected (OHD) optical Kerr effect detection scheme[6] is inherently limited to measurements of the anisotropic portion of the Raman scattering polarizability tensor (or equivalently response function). Several methods have been demonstrated for the observation of polarization specific responses based on either active or passive phase locked local oscillator pulse schemes or Z-scan based analysis.[7–13] Since distinct scattering or relaxation mechanisms may dominate different portions of the Raman polarizability tensor, the observation of polarization specific Raman responses provides some ability to distinguish these different sources of Raman activity. Such identification, particularly when accompanied by theoretical models, such as equilibrium[14] and finite field[15] molecular dynamics simulations, and instantaneous normal mode (INM) calculations[16], offers molecular based descriptions of the nature of these intermolecular responses.

We have recently demonstrated an alternative two beam pump-probe technique based on the observation of frequency selected portions of the nominally putative dichroic response of transparent liquids for the observation of polarization specific ultrafast responses.[17] By viewing a frequency selected portion of the dichroic signal pulse, the nearly complete cancellation of signal intensity on the two sides of the probe pulse spectrum is avoided and a robust dichroic response may be readily observed. In liquid CS_2 the decay of the isotropic Raman response is found to be dominated by an ~0.5 ps decay.[13,17] The corresponding anisotropic decay exhibits a decay constant due to diffusive reorientation at long times but also contains this same ~0.5 ps decay component.[18] Based on the results of INM calculations, this decay was attributed to the frequency inhomogeneity of the distribution of the intermolecular Raman active modes of CS_2.[17]

Aside from the observation of decay time scales, the more complete analysis of polarization specific Raman responses requires the recovery of the nuclear impulse response function, at least within the frequency regime of the incident pulses. For birefringence based techniques, this is readily accomplished by a normalization procedure utilizing the pulse autocorrelation as first developed by McMorrow and Lotshaw.[19] In our previous work,[17] we briefly indicated how the nuclear response function could be obtained for this dispersed dichroic technique. Here, we show a preliminary attempt to recover the nuclear impulse response function of liquid CCl_4 via this procedure.

The role of so-called coherence coupling terms can complicate the analysis of electronically resonant pump–probe responses and has been explored by several investigators.[1,20–26] Such contributions arise only when pump and probe pulses are temporally overlapped and result from field interaction histories where a probe field interaction precedes either the first or second pump field interaction with the medium. The contribution of these non-sequential pump–probe terms has even been employed as a measure of optical coherence decay times for electronically resonant samples.[22,24,26] The effects of such coherence coupling field time evolution histories for electronically nonresonant samples has been explicitly considered less often.[3,27,28] Here we explore the consequences for this contribution to the third-order polarization pump–probe signal in electronically (both in a one and two photon sense) nonresonant media. The effects of these coherence coupling terms are considered for both the standard frequency integrated birefringence and dichroic responses as well as the dispersed dichroic signals proposed[17] for polarization specific Raman spectral density measurements.

Theoretical Description

Nondispersed Pump–Probe Responses of Transparent

Materials. The two-beam optical heterodyne detected (OHD) signal due to the third-order polarization response of a sample as a function of time delay, τ, between pump and probe pulses is given by[1]

$$S_{ijkl}(\tau) = -2\mathrm{Im}\left[e^{-i\theta}\int_{-\infty}^{\infty}\hat{E}_i^{*pr}(t)\hat{P}_{ijkl}^{(3)}(t,\tau)\right] \quad (1)$$

where, the idices i, j, k, l, correspond to the polarization directions, in the lab fixed frame, of the time-ordered, active electric fields (reading temporally from right to left). Dichroic ($\theta = 0$) and birefringent ($\theta = \pi/2$) signals result from control over the relative phase between the final probe pulse field (local oscillator) and the $P^{(3)}$ generated signal field.

The total observed signal predicted by Eq. 1, results from a sum over all possible radiation field time orderings consistent with the wavevector phase-matching conditions for a given experimental configuration. $\hat{P}_{ijkl}^{(3)}(t,\tau)$ is derived from the corresponding third order impulse response function, $R_{ijkl}^{(3)}(t)$. Within a Born–Oppenheimer description of molecular states, this response function, which in general is a complex function, may be written as a sum of contributions from electronic (e) and nuclear (n) degrees of freedom: $R_{ijkl}^{(3)} = R_{ijkl}^{(3e)} + R_{ijkl}^{(3^n)}$. When the incident frequencies are not coincident with any regions of one- or two-photon electronic absorption, the corresponding nonresonant electronic response can be taken to be instantaneous and proportional to a real constant.[29] Thus for such transparent samples

$$R_{ijkl}^{(3)}(\tau') = \gamma_{ijkl}\delta(\tau') + R_{ijkl}^{(3n)}(\tau') \quad (2)$$

In general there are two types of time-evolution histories which can contribute to pump-probe experiments.[1] These contributions differ only in the temporal order of electric field interactions that account for the third order polarization. They are described as sequential and coherent coupling terms and are defined below for two beam, one color experiments.

$$\hat{P}_{jjkk}^{(3n)seq}(t,\tau) = \hat{E}_j^{pr}(t-\tau)\int_{-\infty}^{\infty}d\tau'\hat{E}_k^{*pu}(t-\tau')\hat{E}_k^{pu}(t-\tau')R_{jjkk}^{(3n)}(\tau') \quad (3a)$$

$$\hat{P}_{jkkj}^{(3n)coh}(t,\tau) = \hat{E}_k^{pu}(t)\int_{-\infty}^{\infty}d\tau'\hat{E}_k^{*pu}(t-\tau')\hat{E}_j^{pr}(t-\tau-\tau')R_{jkkj}^{(3n)}(\tau') \quad (3b)$$

$$\begin{aligned}\hat{P}_{jkkj}^{(3e)coh}(t,\tau) &= \hat{E}_k^{*pu}(t)\int_{-\infty}^{\infty}d\tau'\hat{E}_k^{pu}(t-\tau')\hat{E}_j^{pr}(t-\tau-\tau')R_{jkkj}^{(3e)}(\tau') \\ &= \gamma_{jkkj}\hat{E}_k^{*pu}(t)\hat{E}_k^{pu}(t)\hat{E}_j^{pr}(t-\tau)\end{aligned} \quad (3c)$$

$\hat{E}_j^{\alpha}(t)$ is the pulse envelop of the pump or probe ($\alpha = pu, pr$) fields centered at carrier frequency Ω. The Eq. 3 signal polarizations are given explicitly for the two pump pulse and the two probe pulse interaction to be polarized along the same direction. As seen above, the coherence coupling terms contribute only when the pulses overlap. Phase matching constrains the nonresonant electronic contribution to a coherent coupling history only (Eq. 3c). The third-order nuclear impulse response function is formally described in terms of the two-time correlation function of the transition polarizability by: $R_{ijkl}^{(3n)}(t) = i/h\langle[\alpha_{ij}(t), \alpha_{kl}(0)]\rangle$.[1]

The effects of the coherence coupling term arising from two distinct types of impulse nuclear response functions ($R^{(3n)}(t) = \sin\omega t \exp(-t/T_2)$) alone are illustrated in Fig. 1. The birefringent and dichroic coherence coupling signals due to an all real nuclear impulse response function given by an overdamped ($\omega = 12.5$ cm^{-1}, $T_2 = 0.12$ ps) and an underdamped ($\omega = 400$ cm^{-1}, $T_2 = 1$ ps) response, respectively, are compared in Figs. 1a and 1b for 45 fs Gaussian pulses with transform limited bandwidth, i. e. non-chirped pulses. The shape of the birefringent coherent coupling signal is identical to that of the pulse autocorrelation function and the corresponding dichroic response vanishes for nonchirped pulses regardless of the time scale of the nuclear impulse response function. However, when the 45 fs pulses are linearly chirped, as illustrated in Figs. 1c and 1d for Gaussian pulses that have 1.3 times the transform limited bandwidth, the coherence coupling dichroic responses have a dispersive lineshape[30] and the corresponding birefringent response is narrower than the pulse autocorrelation. These responses are dependent on the nature of the nuclear response function at least for the limits of overdamped and underdamped nuclear response functions tested here (see Figs. 1c and 1d).

In Fig. 2 the relative importance of the coherence coupling term to the total calculated birefringent responses are shown for these two types of nuclear response functions (overdamped and underdamped). As seen in Figs. 2a and 2b, the relative contribution of the coherence coupling term to the total (coherence coupling plus sequential) response is much larger for the underdamped nuclear impulse response function. This arises from the larger overlap between the nuclear impulse response function and the pulse envelopes for the higher frequency components at the smallest delay times.

A less obvious feature regarding these coherence coupling effects is illustrated in the lower panels of Fig. 2. For the two nuclear impulse response functions illustrated in Fig. 2c, the corresponding total (coherence coupling plus sequential) birefringent responses are shown in Fig. 2d for 45 fs pulses. The overdamped response function (solid line Fig. 2c) is the same as described above (Fig. 2b). The birefringent response given by the dashed line in Fig. 2d, results from a nuclear impulse response function which has the same overdamped component plus a high frequency (668 cm^{-1}) underdamped mode (Fig. 2c). This frequency is outside the width of a 45 fs pulse (FWHH 360 cm^{-1}). The calculated birefringent signals *beyond* the pulse overlap region are virtually identical for each of these nuclear impulse response functions and 45 fs pulses. However, the coherence coupling signal derived from the nuclear impulse response function with the additional high frequency component is greatly enhanced even though it is barely detectable in the signal due to the sequential field history as seen in Fig. 2d.

These nuclear response simulations clearly indicate that judging the relative magnitudes of the electronic and nuclear contributions exclusively on the basis of the relative intensity of an autocorrelation like feature at $\tau = 0$ can be in error due to these coherence coupling terms derived from $R^{(3n)}(t)$. Furthermore, modes that are invisible to the sequential birefringent signal will also contribute to this coherence coupling effect.

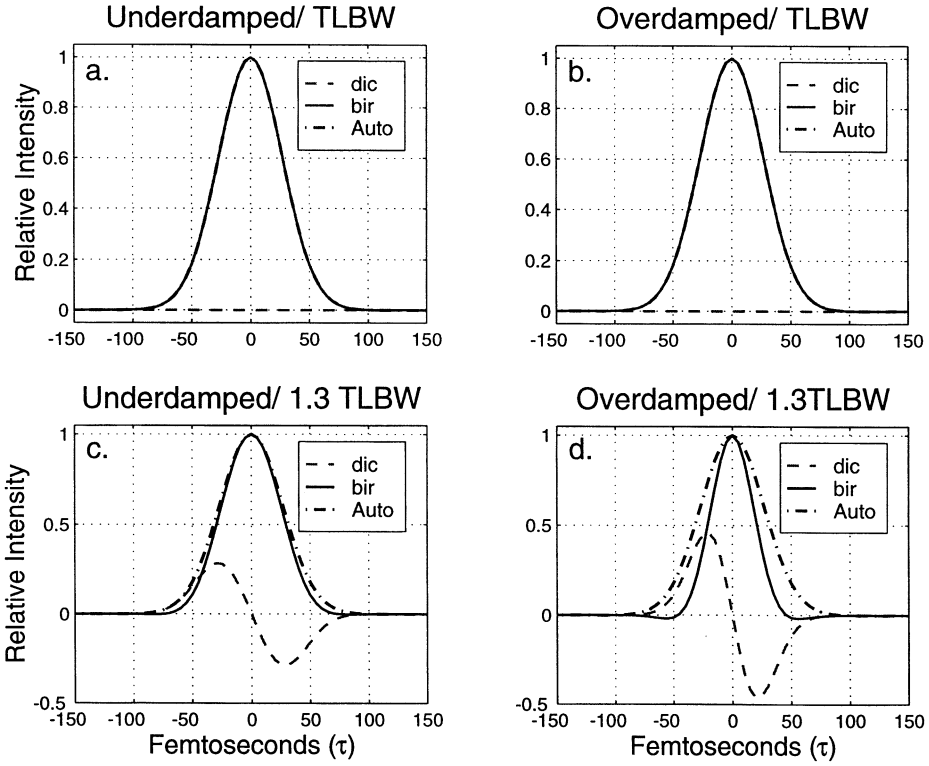

Fig. 1. Coherent coupling contribution to birefringent and dichroic responses derived from an (a) underdamped ($R^{(3)}$ = sin (400 $cm^{-1}\tau$)exp($-\tau$/800 fs)) and (b) overdamped ($R^{(3)}$ = sin (12.5 $cm^{-1}\tau$) exp($-\tau$/120 fs)) nuclear response function and 45 fs Gaussian pulses are compared to the pulse autocorrelation function. The same comparison is shown in (c) and (d) for linearly chirped 45 fs pulses with 1.3 times the transform limited bandwidth (TLBW).

However, the contribution of these coherent coupling signals will have no effect on the spectral densities recovered from birefringence measurements due to the symmetry of the birefringent coherent coupling responses (Fig. 1). The now standard procedure for normalizing observed birefringent responses for finite pulse duration and thereby generating the nuclear impulse response function, is to take the *imaginary* part of the quotient of the Fourier transforms of the observed birefringence signal and the pulse autocorrelation.[19] This procedure has the added benefit of eliminating the coherent coupling contribution due to the nuclear response function as well the nonresonant electronic contribution on the basis of symmetry.

Dispersed Pump–Probe Dichroic Responses of Transparent Materials. The dispersed optical heterodyne detected birefringent or dichroic response as a function of interpulse delay, τ, and the selected probe pulse frequency, Δ_D, is given by[1,31]

$$S_{ijkl}(\Delta_D,\tau) = -2\mathrm{Im}\left[e^{-i\theta}\tilde{E}_i^{*pr}(\Delta_D)\tilde{P}^{(3)}_{ijkl}(\Delta_D,\tau)\right] \quad (4)$$

Δ_D is the detuning of the detected probe pulse frequency, ω_D, from the carrier frequency of the probe pulse (Ω), i. e. $\Delta_D = \Omega - \omega_D$. $\tilde{P}^{(3)}_{ijkl}(\Delta_D,\tau)$ is the Fourier transform of the third-order polarization response of the material,

$$\tilde{P}^{(3)}_{ijkl}(\Delta_D,\tau) = \frac{1}{\sqrt{2\pi}}\int_{-\infty}^{\infty} dt \exp(-i\Delta_D t)\hat{P}^{(3)}_{ijkl}(t,\tau) \quad (5)$$

and, correspondingly, $\tilde{E}_i^{*pr}(\Delta_D)$ is proportional to the Fourier transform, i.e. spectrum, of the probe field

$$\tilde{E}_i^{*pr}(\Delta_D) = \frac{1}{\sqrt{2\pi}}\int_{-\infty}^{\infty} dt \exp(i\Delta_D t)\hat{E}_i^{*pr}(t-\tau) \quad (6)$$

The sequential pump-probe dichroic response due to an all real nuclear impulse response function vanishes when all probe frequencies are detected.[17] However, we have previously shown that for such nonresonant, i. e. transparent media, a significant dichroic pump-probe response can be observed when only a frequency selected portion, on one side of the probe pulse spectrum, is detected.[17] This frequency selected dichroic technique thus allows the observation of polarization specific responses for transparent materials with a simple variation of the standard two beam setup. Placement of a filter that transmits a portion of the probe pulse spectrum before detector allows the observation of these polarization specific dichroic responses.

The impulse response function can be recovered from the frequency selected *sequential* contribution, which dominates the response when the pulses are no longer overlapped, when the corresponding frequency selected purely electronic response is observed under the same experimental conditions. The impulse response function is then formally given by[17]

$$R^{(3n)}(\omega) = -\mathrm{Im}\,\Im\{R^{(3n)}(\tau)\} = -\mathrm{Im}\left[\frac{\Im\{S(\Delta_D,\tau)\}}{\Im\{S_{el}(\Delta_D,\tau)\}}\right] \quad (7)$$

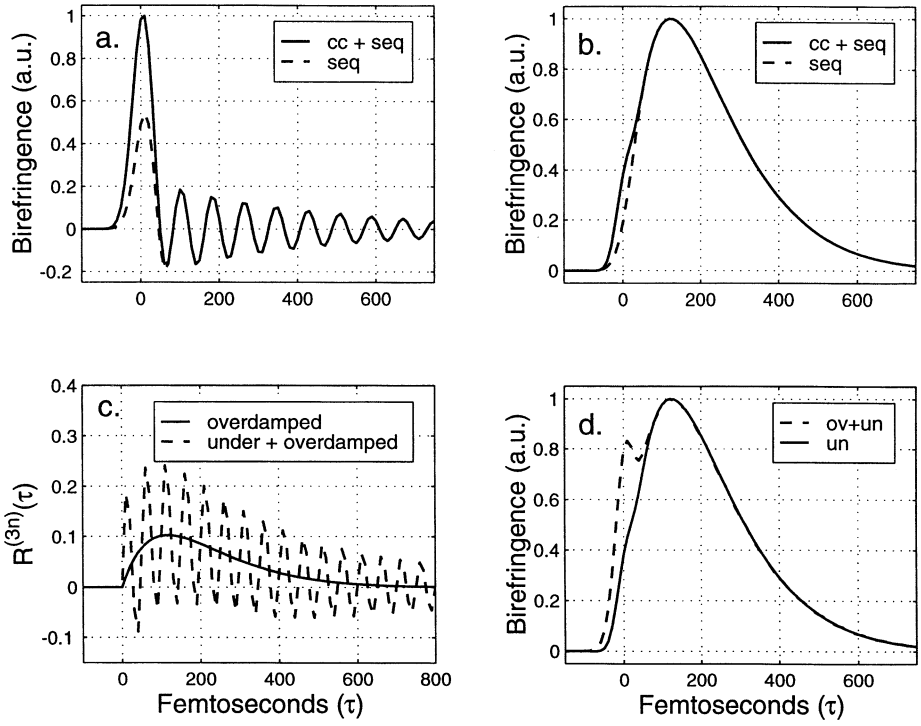

Fig. 2. (a) The birefringence due to both sequential (seq) and coherence coupling (cc) terms for an underdamped nuclear response function ($R^{(3)}$ = sin (400 cm$^{-1}\tau$)exp($-\tau$/800 fs)) and 45 fs Gaussian pulses. (b) Same as in (a) for an overdamped nuclear response function ($R^{(3)}$ = sin (12.5 cm$^{-1}\tau$) exp($-\tau$/120 fs)). (c) Two nuclear response functions are shown. The solid line is the overdamped response function described above. The dashed line corresponds to a response function that is a sum of the overdamped response and an additional overdamped mode contribution ($R^{(3)}$ = sin (12.5 cm$^{-1}\tau$) exp($-\tau$/120 fs) + 0.15sin (668 cm$^{-1}\tau$)exp($-\tau$/800 fs). (d) The total (coherence coupling and sequential) calculated birefringent response due to 45 fs Gaussian pulses and the two response functions given in 2c are shown.

The operator, $\Im$, corresponds to Fourier transform with respect to τ. $S(\Delta_D, \tau)$ and $S_{el}(\Delta_D, \tau)$ are the observed frequency selected dichroic (or birefringent) sample and electronic only responses respectively. When the numerator and denominator in Eq. 7 are summed first over all frequencies, Δ_D, the usual statement about the recovery of the nuclear spectral density[19] is obtained. This expression is exact for chirped or nonchirped pulses and holds as long as homodyne ($|P^{(3)}|^2$) and any other higher contributions can be neglected. The frequency selected purely electronic response required for the implementation of this procedure, $S_{el}(\Delta_D, \tau)$, may be obtained by repeating the measurement with a material that has only a putative nuclear response such as quartz. The effects of coherence coupling terms on this Fourier transform recovery scheme will be considered below. This method will be tested initially here by the polarization responses of CCl_4 liquid.

Results and Discussion

Experimental Summary. Details of the experimental procedure and setup have been described previously.[17] Briefly, these responses were obtained with 50 fs pulses with ~1.25 transform limited bandwidth centered at 600 nm. A Schott RG610 red transmitted cutoff filter was placed between the sample and detector in the probe beam path. Polarizations of the pump and probe beams were controlled by $\lambda/2$ plate/polarizer combinations. Spectroscopic grade CCl_4 was flowed through a 1 mm path length quartz cell. A 1 mm thick suprasil quartz plate was used to obtain the corresponding electronic response.

Polarization Considerations. In an isotropic medium there are only four nonzero third order response functions and they obey the well-known relationship:[32] $R^{(3)}{}_{ZZZZ} = R^{(3)}{}_{ZZXX} + R^{(3)}{}_{ZXZX} + R^{(3)}{}_{ZXXZ}$. For (electronically) nonresonant Raman transitions, $R^{(3n)}{}_{ZXZX} = R^{(3n)}{}_{ZXXZ}$, and consequently there are only two linearly independent polarization specific polarizability/scattering components. These components are often recast in terms of the trace and traceless symmetric portions of the scattering tensor, i. e. the isotropic and anisotropic response functions, $R^{(3n)}{}_{iso}$ and $R^{(3n)}{}_{aniso}$. The experimentally observed polarization orientations are given by: $R^{(3n)}{}_{ZZZZ} = 4/3\ R^{(3n)}{}_{aniso} + R^{(3n)}{}_{iso}$, $R^{(3n)}{}_{zzxx} = R^{(3n)}{}_{iso} - 2/3\ R^{(3n)}{}_{aniso}$ and $R^{(3n)}{}_{ZZmm} = R^{(3n)}{}_{iso}$, in terms of these two components. The *m* subscript designation corresponds to the magic angle orientation (54.7°) of pump and probe pulses and the resulting (sequential) signal is exclusively derived from the isotropic portion of the scattering tensor/response function.

Dispersed Dichroic Responses. The polarization specific frequency selected dichroic responses of liquid CCl_4 are shown in Fig. 3 for the parallel, perpendicular and magic angle relative polarization orientations of pump and probe pulses. CCl_4 has three low frequency intramolecular Raman active modes at 218 cm^{-1}, 313 cm^{-1}and 459 cm^{-1} that can be impulsively excited by ultrafast pulses. The 218 cm^{-1} and 313 cm^{-1} modes are nontotally symmetric and hence are derived, only

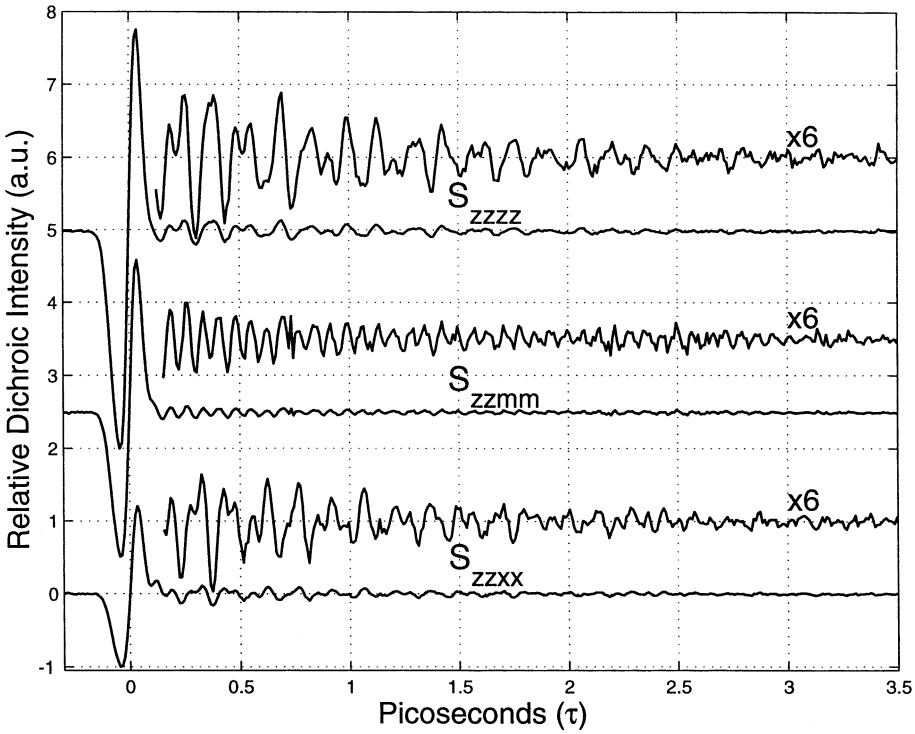

Fig. 3. Observed frequency selected dichroic responses of CCl_4 obtained with 50 fs pulses at 600 nm. Pump and probe pulse relative polarizations are indicated for each response. m corresponds to magic angle orientation. Responses are offset by 2.5 units to facilitate viewing.

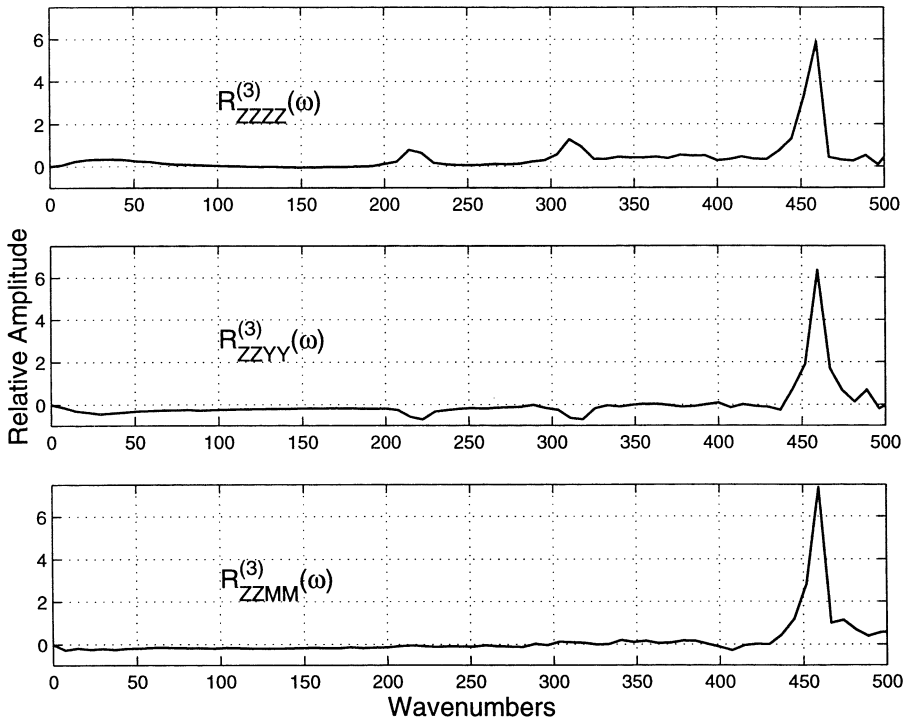

Fig. 4. Spectral densities recovered by procedure described in the text (Eq. 7) for each of the observed partially integrated polarization specific dichroic responses shown in Fig. 3.

from the anisotropic part of the polarizability response function. The 459 cm^{-1} band, in contrast, is a totally symmetric mode which, by symmetry in the T_d group, is derived exclusively from the isotropic part only of the Raman response function.

The corresponding nuclear spectral densities, determined by

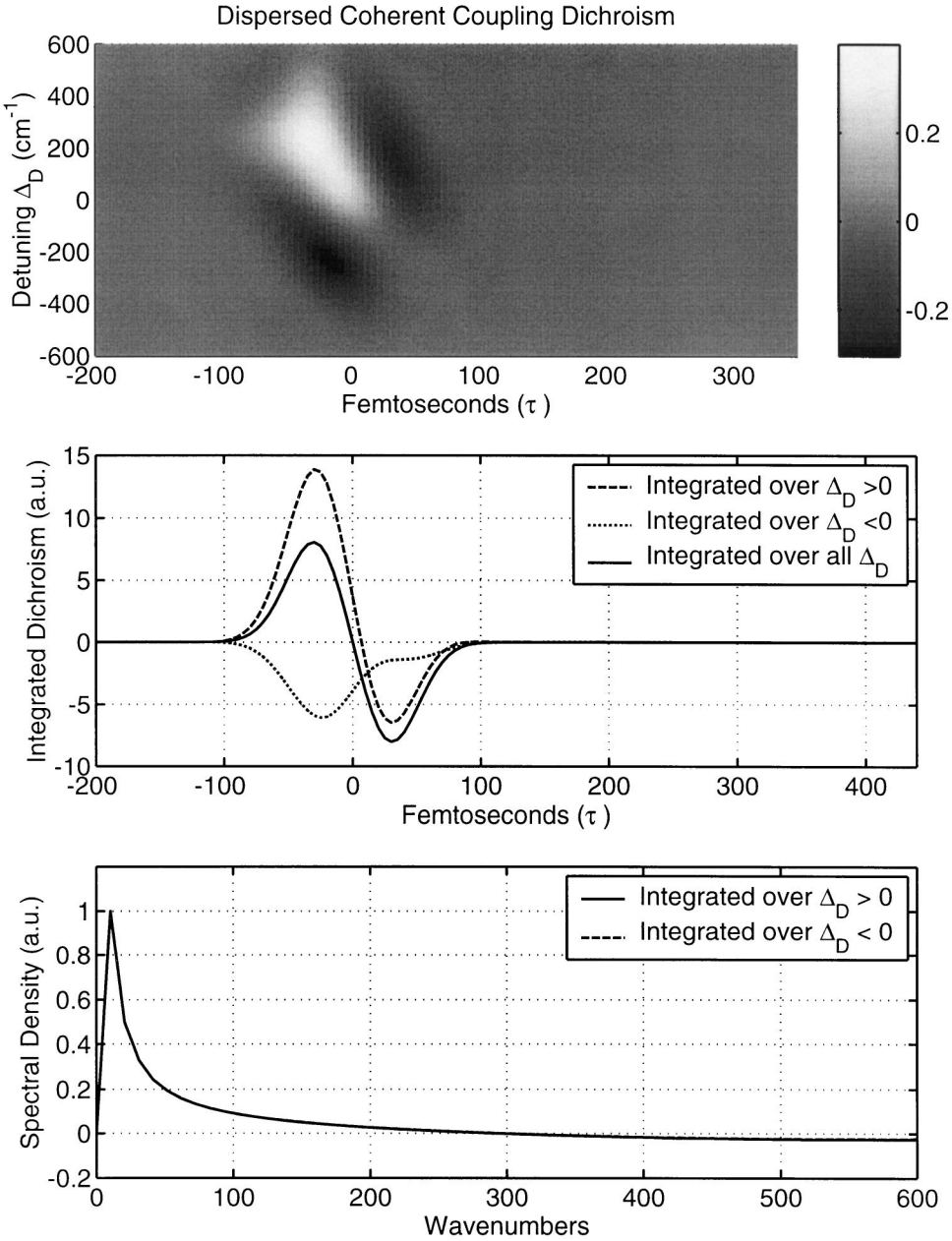

Fig. 5. Dispersed dichroic coherence coupling response due to a nuclear impulse response function of the form: $R^{(3n)}(t) = \sin 459\ \mathrm{cm}^{-1} t \exp(-t/1\ \mathrm{ps})$ for 45 fs Gaussian pulses (1.2 transform limited bandwidth) is shown in the upper panel. The corresponding dispersed dichroic signal is integrated over all the probe frequencies or half the probe frequencies in the middle panel. The spectral density determined by Eq. 7 for this partially integrated dichroic coherence coupling response.

the quotient given in Eq. 7, are shown in Fig. 4. The purely electronic response required for the recovery of the spectral density was obtained by replacing the CCl_4 sample cell with a piece of suprasil quartz. The nuclear response of quartz is quite weak in comparison with the nonresonant electronic portion of the response at least for pulses of 40 fs or greater and is hence used in pulse characterization procedures (e. g. PG FROG[33]). As seen in this figure this spectral density recovery scheme appears to do a reasonably good job of recovering the polarization specific spectral densities. For example the relative amount of isotropic component should be the same in each response, the depolarized modes at 218 cm^{-1} and 313 cm^{-1} should be of opposite sign in the $R_{zzzz}^{(3)}$ and $R_{zzxx}^{(3)}$ polarizability elements and a factor of two different in intensity. In addition, a weaker low frequency ($< 100\ cm^{-1}$) component, corresponding to the intermolecular Raman response of CCl_4 is also evident in the experimental responses containing the anisotropic scattering component and shows the same sign changing behavior as the two depolarized intramolecular modes. These observations are in agreement with the polarization considerations described above and previous results.[8,10]

However, some discrepancies between the recovered Raman spectral densities reported here and those published previously are evident.[8,10] In particular, the spectral density associated

with the intermolecular modes rises too slowly at the low frequency end and the relative intensity of the 218 and 313 cm^{-1} modes appears somewhat too small in the recovered spectral density. Furthermore, the baselines (Fig. 4) of the spectral densities could not be flattened by simply shifting the $t = 0$ point. We attribute these errors in the implementation of the spectral density recovery procedure outlined above (Eq. 7) predominantly to the effects of dispersed coherence coupling terms derived from the nuclear response function contributions to the observed responses. These terms will appear both in the dispersed response of the sample (numerator Eq. 7) and potentially, in the dispersed response of the electronic only normalization response (denominator Eq. 7).

As an example of the kind of distortion that may arise in the spectral density recovered from (one color) dispersed dichroisms, the calculated dichroic response due to the coherence coupling term derived from a response function of the form $R^{(3n)}{}_{(t)} \sim \sin(459\ cm^{-1})t \exp(-t/1.1ps)$ and 45 fs Gaussian pulses with 1.2 transform limited bandwidths, are shown in Fig. 5 (upper panel) as a function of τ and Δ_D. In the middle panel the coherence coupling dichroic signals integrated over all the probe frequencies or integrated over just half the probe pulse spectrum are displayed. The effective spectral density contributed by this history of field interactions determined by implementing the normalization indicated in Eq. 7 is given in the lower panel of Fig. 5. As evident here the coherent coupling terms will contribute some low frequency distortions as well as alter the baseline to these deconvoluted responses. The exact appearance of these coherence coupling terms in the determined nuclear spectral density is difficult to quantitatively estimate since these terms can affect both the normalizing "purely" electronic dispersed response and the dispersed sample signal. This distortion will also be dependent on the precise chirp characteristics of the pulses and the detected frequencies. As shown in Fig. 1, the integrated dichroic response vanishes for nonchirped pulses and purely real response functions.

Furthermore, for a sequential contribution that is derived from the $R^{(3n)}{}_{ijkl}$ impulse response function, the overlapping coherence coupling contribution will be determined by the $R^{(3n)}{}_{ikjl}$ and $R^{(3n)}{}_{iklj}$ polarizability responses. Thus except for the all parallel polarized configuration R_{zzzz}, the coherence coupling term will be driven by different combinations of isotropic and anisotropic scattering than the sequential response. For example, for the magic angle observation the sequential features are controlled by $R^{(3n)}{}_{zzmm} = R^{(3n)}{}_{iso}$. In contrast, the corresponding nuclear coherence coupling contribution is derived from $R^{(3n)}{}_{zmzm} = R^{(3n)}{}_{iso}/3 + 10R^{(3n)}{}_{aniso}/3$.[34] Thus, in order to insure that these coherence coupling terms do not distort the nuclear spectral densities recovered via this frequency selected dichroic technique, *this procedure must be carried out on nonresonant responses obtained with different color pump and probe pulses*. Due to the mismatch in carrier frequency, the nuclear coherence coupling terms vanish in two color pump-probe responses and hence the interference from this term will no longer be a contributor to this procedure. The mismatch in pulse frequencies (Ω_1–Ω_2) must be sufficient to eliminate finite contributions from the nuclear response formally arising from Eq. 3b, i. e. $|\Omega_1 - \Omega_2| >> \omega_{vib}$.

Conclusions

In order to avoid contamination from coherence coupling effects in the recovery of Raman spectral densities quantitatively via the previously described frequency selected dichroic technique two color pump-probe responses must be obtained. It remains to be demonstrated whether polarization specific responses obtained via these two-color pump probe dichroisms provide additional advantages over passive phase-locked or Z-scan approaches either in terms of ease of implementation or improved dynamic range and signal to noise ratio. Although, the nuclear response function contribution to the coherent coupling signal may distort simple estimates of the relative electronic and nuclear contributions based on the intensity of the "autocorrelation-like" feature around $\tau = 0$, the contribution of this field history to recovered nuclear spectral densities via the (standard) Fourier transform normalization method is vanishing owing to the symmetry of this feature. The dichroic contribution however, derived from this coherence coupling term provides a direct measure of the linear chirp of ultrafast pulses and this diagnostic aspect will be further explored in a future study.

The support of the National Science Foundation and the Boston University Photonics Center are gratefully acknowledged.

References

1 S. Mukamel, "Principles of Nonlinear Optical Spectroscopy," Oxford University Press, New York (1995).

2 S. Ruhman, A. G. Joly, and K. A. Nelson, *J. Chem. Phys.*, **86**, 6563 (1987).

3 D. McMorrow, W. T. Lotshaw, and G. A. Kenney-Wallace, *IEEE J. Quant. Electron.*, **24**, 443 (1988).

4 M. Cho, M. Du, N. F. Scherer, G. R. Fleming, and S. Mukamel, *J. Chem. Phys.*, **99**, 2410 (1993).

5 L. D. Ziegler, R. Fan, A. E. Desrosiers, and N. F. Scherer, *J. Chem. Phys.*, **100**, 1823 (1994).

6 G. L. Eesley, M. D. Levenson, and W. M. Tolles, *IEEE J. Quantum Electron.*, **14**, 45 (1978); M. D. Levenson and G. L. Eesley, *Appl. Phys.*, **19**, 1 (1979).

7 P. Cong, Y. J. Chang, and J. D. Simon, *J. Phys. Chem.*, **100**, 8613 (1996); Y. J. Chang, P. Cong, and J. D. Simon, *J. Chem. Phys.*, **106**, 8639 (1997).

8 S. Matsuo and T. Tahara, *Chem. Phys. Lett.*, **264**, 636 (1997).

9 G. Goodno, G. Dadusc, and R. J. Dwayne Miller, *J. Opt. Soc. Am. B*, **15**, 1791 (1998).

10 M. Khalil, O. Golonzka, N. Demirdoven, C. J. Fecko, and A. Tokmakoff, *Chem. Phys. Lett.*, **321**, 231 (2000).

11 M. Khalil, N. Demirdoven, O. Golonzka, C. J. Fecko, and A. Tokmakoff, *J. Phys. Chem. A*, **104**, 5711 (2000).

12 J. A. Gardecki, G. Yu, S. Constantine, J. Peng, Y. Zhou, and L. D. Ziegler, *J. Chem. Phys.*, **114**, 3586 (2001).

13 Q.-H. Xu, Y.-Z. Ma, and G. R. Fleming, *Chem. Phys. Lett.*, **338**, 254 (2001).

14 For example: L. C. Geiger and B. M. Ladanyi, *J. Chem. Phys.*, **87**, 199 (1987).

15 T. I. C. Jansen, J. G. Snijders, and K. Duppen, *J. Chem.*

Phys., **113**, 307 (2000).
16 R. L. Murry, J. T. Fourkas, and T. Keyes, *J. Chem. Phys*., **109**, 2814 (1998).
17 S. Constantine, J. A. Gardecki, Y. Zhou, L. D. Ziegler, X. D. Ji, and B. Space, *J. Phys. Chem. A*, **105**, 9851 (2001).
18 B. J. Loughnane, A. Scodinu, R. A. Farrer, and J. T. Fourkas, *J. Chem. Phys*., **111**, 2686 (1999).
19 D. McMorrow and W. T. Lotshaw, *J. Phys. Chem*., **95**, 10395 (1991); *Chem. Phys. Lett*., **174**, 85 (1990).
20 J.-L. Oudar, *IEEE J. Quant, Electron*., **19**, 713 (1983).
21 S. L. Palfrey and T. F. Heinz, *J. Opt. Soc. Am. B*, **2**, 674 (1985).
22 M. W. Balk and G. R. Fleming, *J. Chem. Phys*., **83**, 4300 (1985).
23 W. T. Pollard, S.-Y. Lee, and R. A. Mathies, *J. Chem. Phys*., **92**, 4012 (1990).
24 M. Chachisvilis, H. Fidder, and V. Sundstrom, *Chem. Phys. Lett*., **234**, 141 (1995).
25 P. Cong, H. P. Deuel, and J. D. Simon, *Chem. Phys. Lett*., **212**, 367 (1993).
26 P. Cong, Y. J. Yan, H. P. Deuel, and J. D. Simon, *J. Chem. Phys*., **100**, 7855 (1994).
27 Y. Zhou, S. Constantine, J. A. Gardecki, and L. D. Ziegler, *Chem. Phys. Lett*., **314**, 73 (1999).
28 T. Hattori, A. Terasaki, T. Kobayashi, T. Wasa, A. Yamada, and H. Sasabe, *J. Chem. Phys*., **95**, 937 (1991).
29 R. W. Hellwarth, *Prog. Quant. Electron*., **5**, 1 (1977).
30 L. D. Ziegler and X. Jordanides, (submitted *Chem. Phys. Lett*.).
31 Y. Zhou, S. Constantine, S. Harrel, and L. D. Ziegler, *J. Chem. Phys*., **110**,5893 (1999).
32 M. D. Levenson and S. S. Kano, "Introduction to Nonlinear Laser Spectroscopy," Academic Press (1988).
33 R. Trebino, K. W. DeLong, D. N. Fittinghoff, J. N. Sweetser, M. A. Krumbugel, and B. A. Richman, *Rev. Sci. Instrum*., **68**, 3277 (1977).
34 A. Tokmakoff, *J. Chem. Phys*., **105**, 1 (1996).